Icarus 377 (2022) 114901

Contents lists available at ScienceDirect

Icarus

journal homepage: www.elsevier.com/locate/icarus

Hugoniot and released state of calcite above 200 GPa with implications for hypervelocity planetary impacts

HPSTAR 1431-2022

Yuhei Umeda [a,b,c,d,*], Keiya Fukui [a], Toshimori Sekine [a,e], Marco Guarguaglini [f], Alessandra Benuzzi-Mounaix [f], Nobuki Kamimura [a], Kento Katagiri [a,b], Ryosuke Kodama [a,b], Takeshi Matsuoka [a], Kohei Miyanishi [g], Alessandra Ravasio [f], Takayoshi Sano [b], Norimasa Ozaki [a,b]

[a] Graduate School of Engineering, Osaka University, Osaka, Japan
[b] Institute of Laser Engineering, Osaka University, Osaka, Japan
[c] Institute for Planetary Materials, Okayama University, Tottori, Japan
[d] Institute for Integrated Radiation and Nuclear Science, Kyoto University, Osaka, Japan
[e] Center for High Pressure Science & Technology Advanced Research, Shanghai, China
[f] LULI, CNRS, CEA, Sorbonne Université, École Polytechnique, Institut Polytechnique de Paris, Palaiseau, France
[g] RIKEN SPring-8 Center, Hyogo, Japan

A B S T R A C T

Carbonate minerals, for example calcite and magnesite, exist on the planetary surfaces of the Earth, Mars, and Venus, and are subjected to hypervelocity collisions. The physical properties of planetary materials at extreme conditions are essential for understanding their dynamic behaviors at hypervelocity collisions and the mantle structure of rocky planets including Super-Earths. Here we report laboratory investigations of laser-shocked calcite at pressures of 200–960 GPa (impact velocities of 12–30 km/s and faster than escape velocity from the Earth) using decay shock techniques. Our measured temperatures above 200 GPa indicated a large difference from the previous theoretical models. The present shock Hugoniot data and temperature measurements, compared with the previous reports, indicate melting without decomposition at pressures of ~110 GPa to ~350 GPa and a bonded liquid up to 960 GPa from the calculated specific heat. Our temperature calculations of calcite at 1 atm adiabatically released from the Hugoniot points suggest that the released products vary depending on the shock pressures and affect the planetary atmosphere by the degassed species. The present results on calcite newly provide an important anchor for considering the theoretical EOS at the extreme conditions, where the model calculations show a significant diversity at present.

1. Introduction

Calcite ($CaCO_3$) is known as one of the typical minerals in sedimentary rocks on planetary surfaces of Earth, Mars, Venus, and others (Murchie et al., 2009; Kargel et al., 1994). The presence of carbonates is considered to be evidence of the existence of liquid water, and which was found in the alternating layers of hydrous minerals and clay minerals on the surface of Mars (Murchie et al., 2009). Especially, a lot of carbonates have existed as the marine sediment on the surface of the Earth. Carbonates have also been found in chondritic meteorites, although it is small (1.4–2.8 vol% of CM chondrites) in the total volume (Leuw et al., 2010). Despite that the dynamic behaviors of calcite in hypervelocity impacts are important to understand the shock-induced reactions such as the melting, decomposition, and ionization, the experimental studies are not available yet because the current experimental conditions are limited below about 100 GPa. Reactions of calcite under extreme conditions are required to understand the C/O ratio of stars with hot Jupiter exoplanets (Teske et al., 2014) and the formation process of the atmosphere near stars (Fortney, 2012). When high-speed collisions onto those planetary bodies occur, previous studies indicate that shock-induced reactions of degassing and dehydration produced water and carbon dioxide (Ohno et al., 2008; Kurosawa et al., 2012; Sekine et al., 2015). Such shock-released gases have been considered to play important roles in the atmospheric evolution and ocean formation in planetary history (O'Keefe and Ahrens, 1989).

In the previous studies, Kalashnikov et al. (1973) reported the Hugoniot of calcite at pressures below 95 GPa (at particle velocities of 4 km/s), and shock temperatures were measured up to 160 GPa by Gupta et al. (2002). There are three model calculations on calcite at higher pressures; SESAME (Barnes and Lyon, 1992), ANEOS (Pierazzo et al.,

* Corresponding author at: Institute for Integrated Radiation and Nuclear Science, Kyoto University, Osaka, Japan
E-mail address: umeda.yuhei.2e@kyoto-u.ac.jp (Y. Umeda).

https://doi.org/10.1016/j.icarus.2022.114901
Received 8 June 2021; Received in revised form 25 November 2021; Accepted 14 January 2022
Available online 2 February 2022

1998), and PANDA (Kerley, 1989). A comparison of shock temperatures among the models indicates a significant difference at high pressures. These previous shock pressures were calculated by an extrapolation of the U_s-u_p relation determined below 100 GPa (Kalashnikov et al., 1973). Shock Hugoniot data on calcite are required to simulate more definitively, but currently lacking at pressures above 200 GPa. At such high pressures, most silicates become reflective (e.g, Bolis et al., 2016; Sekine et al., 2016). Recently, the extension and the improvement of their models for silicates such as SiO_2 (Desjarlais et al., 2017; Amodeo et al., 2021) have been starting since the laser shock technique allows us to generate such high pressure-temperature conditions in the laboratory.

Carbonates decompose at high temperatures, but recent high-pressure static experiments and theoretical considerations indicate congruent melting of calcite and aragonite at pressures over ~1 GPa (Spivak et al., 2011; Litvin et al., 2014; Wünnemann et al., 2008). The high-pressure static experiment demonstrated that congruent melting of calcite occurred in pressures of 11–43 GPa and at temperatures of 2000–3400 K (Spivak et al., 2011). With further heating, calcite melts started to decompose above 3400 K (Spivak et al., 2011). Gupta et al. (2002) suggested decomposition of calcite without melting on the Hugoniot based on the shock temperature measurements at pressures over ~100 GPa. However, they used an extrapolated relation of U_s-u_p below 100 GPa by Kalashnikov et al. (1973) to estimate shock pressures. When calcite becomes reflective above 200 GPa in the laser shock compression, we will be able to directly investigate the decomposition or melting of calcite through the Hugoniot measurement although there is no such data for carbonates. Recently the Hugoniot of carbon dioxide has been performed experimentally (Boates et al., 2011; Crandall et al., 2020). A comparison of Hugoniot between calcite and carbon dioxide may shed a light on this problem.

There are several experimental studies on the degassing of carbonates through the shock recovery techniques and in-situ measurements on the shock-compressed carbonates (Ivanov and Deutsch, 2002; Kawaragi et al., 2009; Lange and Ahrens, 1986; Kurosawa et al., 2012). However, the Hugoniot for calcite has not been experimentally investigated at pressures above 100 GPa. The velocity range in the planetary impact in the solar system is expected to be up to 73 km/s taking into account the escape velocity from the Earth (Sekine, 2011). However, most of observed fireballs observed on the Earth are 10 km/s to 30 km/s, although atmospheric deceleration reduces the velocity at the time of impact (Sekine, 2011). Assuming impactors of chondritic meteorites mainly composed of silicates, extreme environments over 200 GPa and over 5000 K are expected at impact velocities over 10 km/s in natural impacts (e.g., Bolis et al., 2016; Sekine et al., 2016; Zhang and Sekine, 2007). For example, it has been known that the Chicxulub impact crater was formed by the asteroid impact with a diameter of ~10 km and an impact velocity of ~20 km/s (Kring, 1995), and this impact occurred in the carbonate-rich environment, and released CO_2 and/or CO that have been proposed as a trigger for mass extinction about 65.5 million years ago (Self et al., 2006). Therefore, the equation of state (EOS) data at pressures over 200 GPa is also essential for the numerical modeling to simulate the chemical effects of crater formation in the large-scale impact phenomena.

In order to depict the chemical effects from shocked carbonates, the estimation of adiabatic temperature from the Huginot state in the impact process is important to understand the impact-induced degassing reactions. When calcite decomposes into CaO and CO_2 at high residual temperature during the release process, the ratio of carbon monoxide to carbon dioxide (CO/CO_2) should be strongly dependent on temperature (Kawaragi et al., 2009). Kawaragi et al. (2009) reported the released gas of CO_2 and CO ($CO/CO_2 = 2.02$) generated by shock-induced reactions that increase 2–5 K in the global terrestrial atmospheric temperature compared with the case of the only CO_2 after the Chicxulub impact (Gulick et al., 2008). CO is known to have more intense, indirect, and radiative forcing than CO_2 owing to the strong greenhouse effect of CH_4 and tropospheric O_3 formed by photochemical reactions (Daniel and Solomon, 1998). If the temperature is extremely high, CO may separate to form free carbon (Litvin et al., 2014). The investigation of the fate of carbonate minerals at extreme conditions is critical to evaluate the greenhouse effect of shock-induced gas and the effects of products on plant and animal life.

Here we report the shock Hugoniot and temperature of calcite at pressures up to 1000 GPa to understand the dynamic behaviors and the shock-induced reactions for applications to the planetary impacts. This is the first experiment for carbonates using the high-power laser, although there are studies on silicates at similar conditions. The adiabatic release temperatures to the ambient condition from three typical Hugoniot states at 100 GPa, 200 GPa, and 300 GPa were calculated to indicate the released gas species.

2. Experimental methods

2.1. Laser shock experiments and optical measurements

The laser shock experiments on calcite were conducted with GEKKO XII laser facility at Osaka University. The GEKKO facility is a neodymium-doped glass laser (the basic wavelength: ω 1053 nm) system. A total of 12 beams (three 2 ω beams with a diameter of 1000 mm and nine 3 ω beams with a diameter of 600 mm) were used in this experiment. The temporal shape of the laser pulse was approximately square with a 2.5 ns duration [full width at half-maximum (FWHM)] and rise and fall times of 100 ps each. We used ~1 cm natural single crystals of calcite $CaCO_3$ (density: 2.71 g/cm^3). Calcite crystals were cut parallel to the cleavage plane. The crystals were polished to be 4 mm square plates (500 μm thick). The target assemblage in the present study is shown in Fig. 1a. All materials of the target were glued with an ultraviolet curing resin.

Shock velocity and thermal emission of the shock wavefront propagating in samples were measured using the velocity interferometer system for any reflector (VISAR) (Barker and Hollenbach, 1972) and streak optical pyrometer (SOP) (Miller et al., 2007; Celliers et al., 2010), respectively. As quartz (Qz) becomes reflective above 150 GPa (Hicks et al., 2006), we can measure the shock velocity as a reference. If calcite becomes reflective at high shock pressure, we can measure both shock velocities on the target simultaneously. The refractive index used in the present study is 1.66 and 1.55 for calcite and Qz, respectively. Velocity sensitivities (velocity per fringe, VPF) of two line-imaging VISARs (line-VISARs) in this study were 7.39 and 4.47 km/s in a vacuum. Based on the Qz Us measured by VISAR, the pressure (P), particle velocity (u_p), and U_s for Alminum (Al) were obtained by the impedance matching for the interface between Al and Qz (Zeldovich and Raizer, 1967). The experimental error of a shock velocity was less than 5% of the velocity sensitivities.

After that, the u_p of calcite was determined by the impedance matching method for the interface between Al and calcite (Celliers et al., 2005). The U_s (km/s) -u_p (km/s) relations used for quartz and Al are $U_s = (6.26 \pm 0.35) + (1.20 \mp 0.02)\ u_p - (2.56 \mp 0.15)\ u_p \exp.[-(0.37 \pm 0.02)\ u_p]$ and $U_s = (6.375 \pm 0.25) + (1.18 \pm 0.03)\ u_p$, respectively (Knudson et al., 2003; Knudson and Desjarlais, 2009). Shock pressure and density (ρ) in calcite were determined from the U_s and u_p using the basic conservation relations (Zeldovich and Raizer, 1967). Uncertainties in the impedance mismatching method were propagated through a Monte Carlo method (Eggert et al., 2008), hence one-sigma uncertainties were taken to be the standard deviation of the distributions. In addition, the reflectivity of shocked calcite was simultaneously obtained from VISAR measurements at the probe laser (532 nm). The reflectivity of shocked Qz was cited from a reference (Celliers et al., 2010).

The SOP measures the thermal emission of the shock front as a function of time and space. The brightness temperature is determined using the gray-body Planck spectrum:

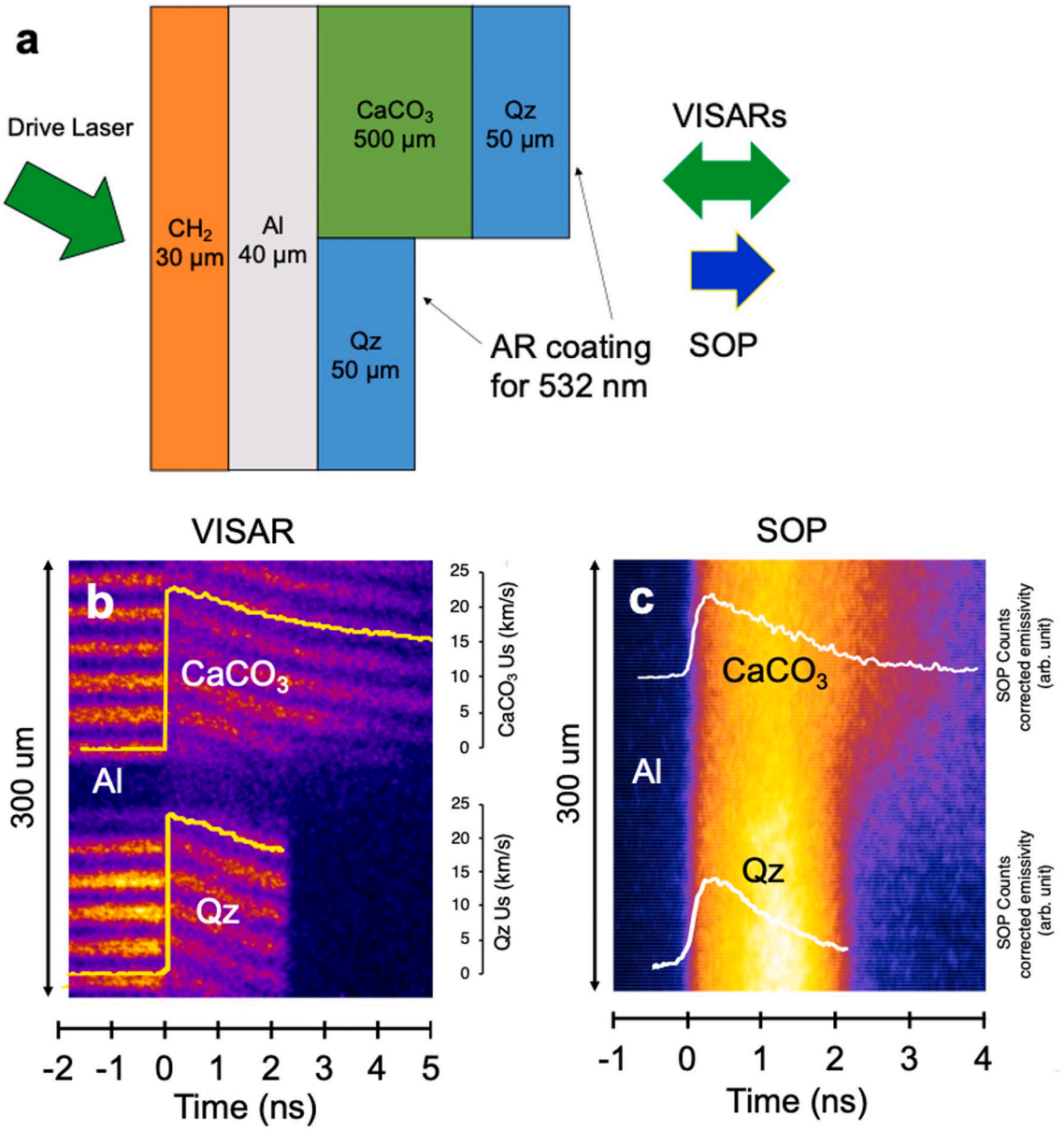

Fig. 1. Schematic setup and typical measurements by VISAR and SOP for shot 42,246 in laser shock experiments. (a) The target assembly consisted of polypropylene (CH_2), aluminum (Al), crystalline α-quartz (Qz), and calcite ($CaCO_3$) from the drive laser side (GEKKO XII). The thickness was 30, 40, 50, and 500 μm for CH_2, Al, Qz, and $CaCO_3$, respectively. The CH_2 was used as an ablator to generate a shock wave, and Al as the base plate, and Qz as the reference material for the impedance mismatching analysis and the temperature determination. The VISAR side of Qz was coated with an anti-reflected (AR) layer for a probe laser at the wavelength of 532 nm. The rear side Qz on calcite was used for the window material since AR coating could not be available for calcite and Qz has almost the same refractive index with calcite. (b) VISAR line-imaging velocity record and inferred shock velocity (yellow curve, scale on right). (c) SOP raw image and count profiles after corrected the emissivity (*1-R*) (white curve). The time zero is set to the arrival time of the shock wave on the Al/$CaCO_3$ and Al/Qz interfaces. The vertical width in images is about 300 μm. (For interpretation of the references to colour in this figure legend, the reader is referred to the web version of this article.)

$$L(\lambda, T) = \varepsilon \frac{2hc^2}{\lambda^5}\left(e^{\frac{hc}{\lambda k_B T}} - 1\right)^{-1} \tag{1–1}$$

where L is the source radiance, h is Planck's constant, c is the speed of light, λ is the wavelength of the radiation, T is the temperature of the Planckian source, K_B is the Boltzmann constant, and ε is the emissivity of the shocked matter. This equation can be reduced to a practical form at the narrow band wavelengths, as described by Miller et al. (2007).

$$T = \frac{T_0}{ln\left(\frac{A\varepsilon}{C} + 1\right)} \tag{1–2}$$

where T_0 and A are calibration parameters that depend on the SOP optical system and C is the CCD (charge-coupled device) counts obtained by the streak camera system. The emissivity ε is calculated from the Kirchhoff law, $\varepsilon = 1 - R$, where R is the shock-front reflectivity. We used quartz as the standard material because the relations between T-U_s and R-U_s have been precisely measured (Hicks et al., 2006; Millot et al., 2015). We determined the value of A from several calibration shots on quartz to measure U_s and SOP simultaneously. More details of the SOP measurement can be found in the previous studies (Sekine et al., 2016; Bolis et al., 2016). The considered error on the temperature is about 15% due to the error on the reflectivity of reference and the temporal resolution of SOP.

2.2. Estimation of an adiabatic release state

The adiabatic release state of shocked calcite is determined to estimate the residual temperature at released pressure. Release isentrope was approximated by using Mie-Grüneisen equation of state (Knudson and Desjarlais, 2013). At first, the following Eq. (2–1) is given by combining the Rankine-Hugoniot equations with the Mie-Grüneisen EOS,

$$P_S(V) = P_H(V)\left[1 - \frac{\Gamma}{2V}(V_0 - V)\right] + \frac{\Gamma}{V}[E_S(V) - E_0] \quad (2\text{–}1)$$

where P, E, and V are the pressure, the internal energy, and the specific volume, respectively. The subscripts H, S, and 0 denote the reference Hugoniot, release adiabat, and the initial state, respectively. Grüneisen parameter Γ was assumed to be a function of V only, using $\Gamma_0 = 0.57$ (Anderson, 2000),

$$\Gamma = \Gamma_0 \frac{V}{V_0} \quad (2\text{–}2)$$

The internal energy on an isentrope was determined by solving the ordinary differential equation (ODE), which gives

$$E_s - E_0 = exp\left[\frac{\Gamma_0}{V_0}(V_1 - V)\right]\left\{\frac{P_1(V_0 - V_1)}{2} - \int_{V_1}^{V} P_H\left[1 - \frac{\Gamma_0}{2V_0}(V_0 - V')\right] \times exp\left[\frac{\Gamma_0}{V_0}(V' - V_1)\right] dV'\right\} \quad (2\text{–}3)$$

where subscript 1 refers to the shocked state. Substituting Eq. (2–3) into Eq. (2–1), we determined the adiabatic release state of calcite using the measured P_1, V_1, and the obtained calcite Hugoniot.

The residual (post-shock) temperature T_2 is given by Eq. (2–4) (Raikes and Ahrens, 1979),

$$T_2 = T_1 exp\left(\int_{V_1}^{V_2} \frac{\Gamma(V')}{V'} dV'\right) \quad (2\text{–}4)$$

where T_1 and V_2 denote the initial shocked temperature and residual specific volume, respectively.

3. Experimental results

Fig. 1b and c show typical data obtained from VISARs and SOP measurements in shot 42246. The calcite becomes reflective above ~200 GPa and for the first time we could measure the physical properties of shock compressed calcite at pressures between 200 and 1000 GPa. Table 1 summarizes the principal Hugoniot results on calcite ($CaCO_3$) as well as quartz (Qz) as the reference. Fig. 2a compares the $U_s - u_p$ relationships between the present and previous studies. The present $U_s - u_p$ relation is approximated by [U_s (km/s) = (3.79 ± 0.33) + (1.26 ± 0.03) u_p] and was used to determine Hugoniot pressure at pressures above 200 GPa. It shows smaller U_s at the same u_p than the SESAME model and is not on the linear extension of the previous low-pressure Hugoniot below 100 GPa (Kalashnikov et al., 1973) [U_s (km/s) = (3.71 ± 0.03) + (1.43 ± 0.01) u_p). The previous results indicate an overestimation by over 10% in pressure above 200 GPa relative to the present U_s-u_p relation. The density in this study is about 0.5 g/cm^3 larger than the SESAME model at ~200 GPa (Fig. 2b). There is a gap at pressures between 100 and 200 GPa, suggesting possible phase change(s) in calcite along the Hugoniot.

The optical reflectivity at 532 nm of calcite along the decaying shock velocity was extracted from VISAR data successfully in three shots. Fig. 3a shows the reflectivity-pressure relations, indicating the onset of reflectivity around 200 GPa probably due to the thermal electron delocalization like silicates (e.g., Sekine et al., 2016; Bolis et al., 2016). The reflectivity profile indicates a large increase at pressures between 350 and 600 GPa (3–30%) and almost saturation above ~800 GPa (>30%). Fig. 3b shows the Hugoniot temperature and a profile in the decaying shock experiment (shot 42246) as a function of pressure, compared with the experimental results up to 160 GPa (Gupta et al., 2002) as well as the results by three models (Barnes and Lyon, 1992, Kerley, 1989; Pierazzo et al., 1998). When the temperature results above 200 GPa are compared with the SESAME model, the difference becomes remarkable (~10000 K at 400 GPa) with increasing pressure.

Table 1
The shock Hugoniot data for calcite ($CaCO_3$) and quartz (Qz).

Shot number	$CaCO_3$ us	$CaCO_3$ u_p	$CaCO_3$ pressure	$CaCO_3$ density	$CaCO_3$ compressiblity	$CaCO_3$ temperature	$CaCO_3$ reflectivity	Qz U_s	Qz u_p
	[km/s]	[km/s]	[GPa]	[g/cm^3]		[K]		[km/s]	[km/s]
42169	13.18 ± 0.22	7.24 ± 0.07	256 ± 3	5.94 ± 0.09	2.19 ± 0.03	–	–	13.62 ± 0.22	7.21 ± 0.11
42180	14.67 ± 0.22	8.68 ± 0.08	341 ± 4	6.57 ± 0.10	2.42 ± 0.04	9250 ± 1120	0.07 ± 0.01	15.58 ± 0.22	8.57 ± 0.11
42184	14.62 ± 0.22	8.50 ± 0.07	333 ± 4	6.40 ± 0.10	2.36 ± 0.04	–	–	15.36 ± 0.22	8.41 ± 0.11
42187	11.6 ± 0.22	6.40 ± 0.10	199 ± 3	5.98 ± 0.10	2.21 ± 0.04	–	–	12.30 ± 0.22	6.32 ± 0.11
42218	18.81 ± 0.22	12.24 ± 0.08	617 ± 5	7.68 ± 0.11	2.83 ± 0.04	–	–	20.23 ± 0.22	12.01 ± 0.12
42220	17.37 ± 0.22	10.40 ± 0.08	484 ± 4	6.68 ± 0.09	2.46 ± 0.03	14760 ± 2210	0.18 ± 0.03	18.00 ± 0.22	10.32 ± 0.12
42223	15.04 ± 0.22	9.05 ± 0.07	365 ± 4	6.73 ± 0.10	2.48 ± 0.04	–	–	16.06 ± 0.22	8.91 ± 0.11
42224	20.03 ± 0.22	12.82 ± 0.08	688 ± 5	7.46 ± 0.10	2.75 ± 0.04	23070 ± 3940	0.28 ± 0.05	21.07 ± 0.22	12.66 ± 0.12
42246	23.22 ± 0.22	15.43 ± 0.08	960 ± 6	7.99 ± 0.10	2.95 ± 0.04	30040 ± 5130	0.38 ± 0.07	24.37 ± 0.22	15.28 ± 0.12
42232	21.02 ± 0.22	13.54 ± 0.08	771 ± 6	7.68 ± 0.10	2.83 ± 0.04	24080 ± 4110	0.31 ± 0.05	22.31 ± 0.22	13.63 ± 0.12

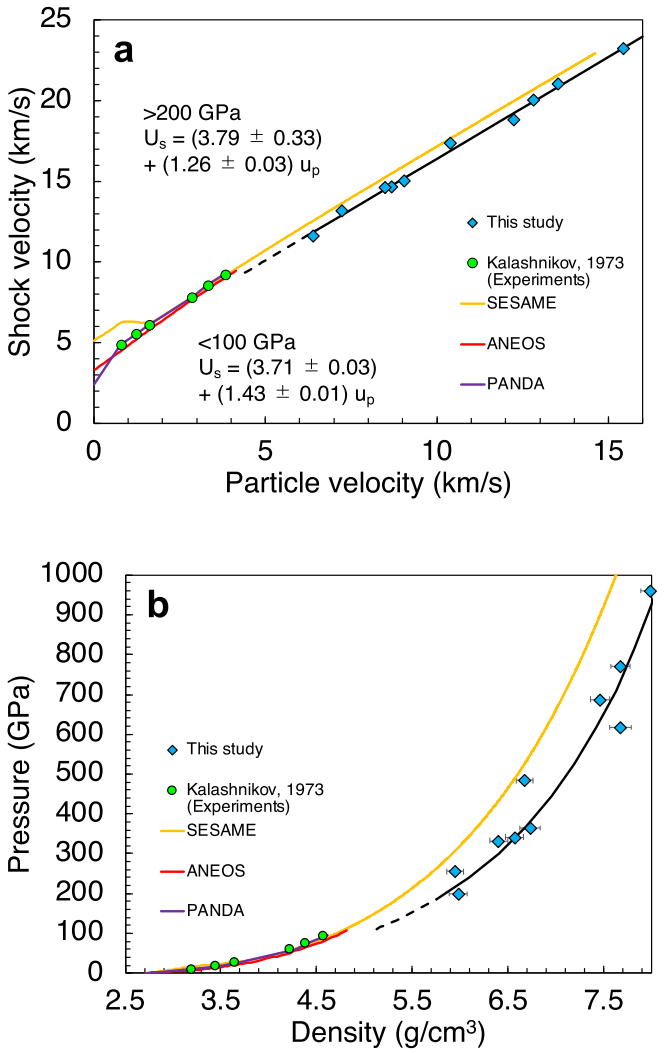

Fig. 2. Hugoniot relations of calcite. (a) The U_s-u_p relations. The present data are shown as light blue diamonds and connected by the solid line of approximation. The dashed line represents the extrapolation of the present study up to the onset of melting (110 GPa). The error bars of this study are smaller than the symbol size. The experimental results by Kalashnikov et al. (1973), and three models by SESAME (Barnes and Lyon, 1992), ANEOS (Pierazzo et al., 1998), and PANDA (Kerley, 1989) are indicated by green circles, and orange, red, and purple solid lines, respectively. (b) The pressure-density relations. The symbols and colors are the same as in Fig. 2a. (For interpretation of the references to colour in this figure legend, the reader is referred to the web version of this article.)

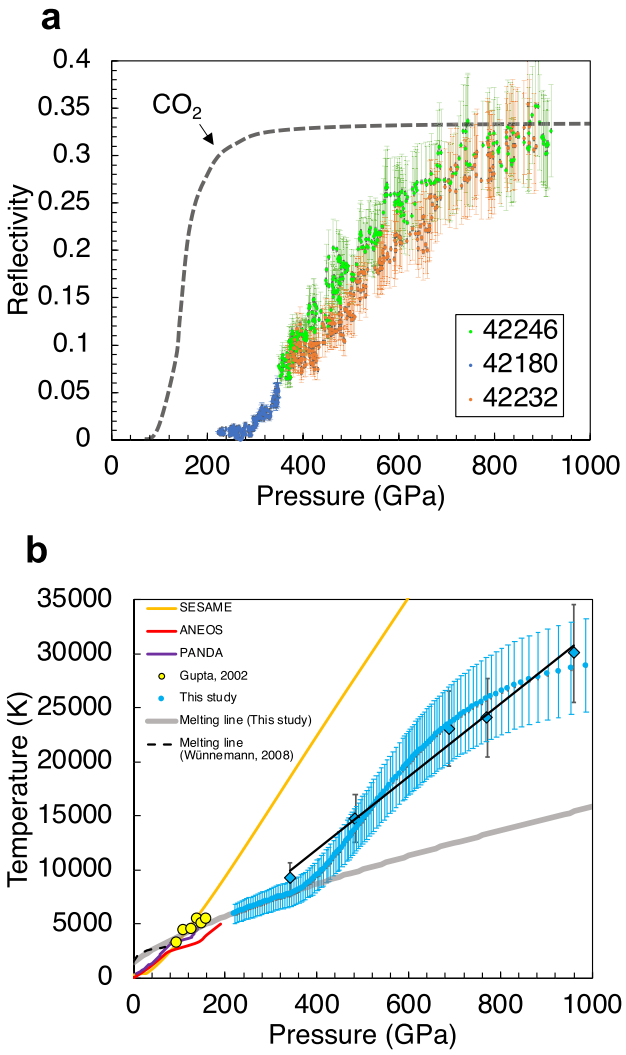

Fig. 3. The reflectivity at 532 nm and temperature of calcite. (a) Reflectivity-pressure relations measured in shots 42246, 42180, and 42232 are shown as the green, blue, and orange plots, respectively and compared with the results on CO_2, as shown by the dotted curve, by Crandall et al. (2020). (b) Measured Hugoniot temperatures (diamonds) and decaying shock profile in shot 42246 (light blue), compared with the previous studies. The black solid line represent the approximation of Hugoniot temperatures of this study. The orange, red, and purple solid lines represent three models of SESAME (Barnes and Lyon, 1992), ANEOS (Pierazzo et al., 1998), and PANDA (Kerley, 1989), respectively. The yellow circles indicate the experimental results (Gupta et al., 2002). The dotted line represents the melting line evaluated at relatively low pressures (Wünnemann et al., 2008). The gray bold line indicates the calcite melting line estimated in the present study using the Simon's equation. (For interpretation of the references to colour in this figure legend, the reader is referred to the web version of this article.)

The adiabatic release state is determined using the Hugoniot data of calcite. The calculation method for the adiabatic release path of pressure and temperature is described in the Method section. The temperatures of calcite released from Hugoniot points are shown as diamonds in Fig. 4a (pink, green, and blue diamonds for 100 GPa, 200 GPa, and 300 GPa, respectively). If T_H (Hugoniot temperature) of calcite is 3500 K at 100 GPa, 6000 K at 200 GPa, and 7000 K at 300 GPa, the corresponding T_R (residual temperature) is 2300 K, 3200 K, and 3600 K at ambient pressure, respectively. At 100 GPa, the SESAME model was used for the calculation. The calculation result on the release state of calcite indicates that the temperatures released at 1 atm (residual temperature) from shock pressures above 100 GPa become much higher than the decomposition temperature of calcite (1200 K at ambient).

4. Discussion

4.1. Hugoniot state of calcite

Fig. 3a and b summarize the profiles of reflectivity and temperature of shocked calcite as a function of pressure during decaying shock and compares with the previous results. The reflectivity of CO_2 at 532 nm rises steeply from ~100 GPa and saturates around 32% from 200 GPa (Crandall et al., 2020). Such tendency is clearly different from our reflectivity profile of calcite (Fig. 3a). The optical reflectivity of CO_2 reveals an insulator-to-conductor transition between 100 and 200 GPa (Crandall et al., 2020). If calcite decomposes into CaO and CO_2 below

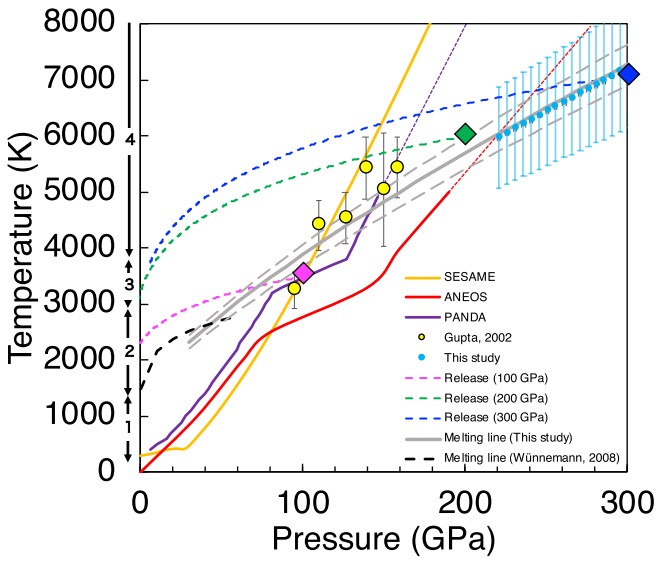

Fig. 4. Pressure-temperature diagram with calculated release adiabats (dotted lines) from Hugoniot state of calcite at 100 GPa (pink), 200 GPa (green), and 300 GPa (blue). The other symbols, colors, and lines are the same as in Fig. 3b. The red and purple dotted lines represent the extrapolation of ANEOS and PANDA models (Pierazzo et al., 1998; Kerley, 1989), respectively, because we don't have the EOS package. The error bar in the melting temperature by the Simon's equation was estimated to be about ±5% (gray dotted lines) based from the 3 point calculations (200, 250, and 300 GPa). The double-headed arrows near zero pressure represent the stable phases at high temperatures; 1 for $CaCO_3$ (solid), 2 for CaO (solid) + CO_2, 3 for CaO (liquid) + CO_2, and 4 for CaO (gas) + CO_2, based on the calcite phase diagram (Ivanov and Deutsch, 2002). (For interpretation of the references to colour in this figure legend, the reader is referred to the web version of this article.)

200 GPa, the reflectivity of calcite may follow that of CO_2. If the decomposition occurs along the Hugoniot, the calculated volume at 200 GPa as a mixture of CaO and CO_2 is 20.0 cm^3/mol (CaO: 9.3 cm^3/mol, CO_2: 10.7 cm^3/mol) using a mixing model based on Hugoniot data for CaO (Jeanloz and Ahrens, 1980) and CO_2 (Crandall et al., 2020). Although the model neglects the temperature difference, this value is significantly greater than the calcite volume of 17.2 cm^3/mol. These comparisons of reflectivity and density between CO_2 and $CaCO_3$ suggest no decomposition of calcite under the Hugoniot state, and are consistent with the previous simulations (Jeanloz and Ahrens, 1980; Boates et al., 2011; Crandall et al., 2020). Previous EOS models differ from the present results. The reason is probable that there was no firm experimental data on decomposition and melting at low pressures at that time.

The previous study on shock temperature measurements on calcite suggested that the onset of the decomposition reaction in calcite to CaO and CO_2 occurs at ~110 ± 10 GPa without melting along the Hugoniot (Gupta et al., 2002) based on the temperature gap between the measured values and the thermodynamic calculation. Taking into account that the gaps are considerably overlapped with the errors (Fig. 4), that pressure was calculated by the low-pressure data by Kalashnikov et al. (1973), and that the temperature reduction by decomposition is ~450 K, the criteria for decomposition and melting may not be firm. Recent static high-pressure experiments and theoretical considerations support congruent melting of calcite and aragonite at high pressures (> ~1 GPa) (Litvin et al., 2014; Spivak et al., 2011; Wünnemann et al., 2008). Therefore, we apply the Simon's equation to evaluate the melting curve of $CaCO_3$. The melting temperature T_m is approximated by the equation. We calculated using the initial point of melting (30 GPa and 2300 K) in the static experiment by Litvin et al. (2014) and our Hugoniot data. P (Pressure, GPa) is applicable above 30 GPa.

$$T_m = T_0\left(\frac{P}{38.30}+1\right)^{0.69}$$

where T_0 is the melt temperature (K) at normal pressure (1500 K), quoted from Irving and Wyllie (1975). The Simon's melting curve is illustrated in Fig. 3b and Fig. 4. It is noteworthy that the data points above 110 GPa by Gupta et al. (2002) are located on or above the curve slightly. Therefore, we consider that calcite melts above a pressure of ~110 GPa. This may correspond to the gap in U_s-u_p (Fig. 2a) between the present results and Kalashnikov et al. (1973). Also, the slopes of the P-T profile between 100 and 150 GPa in PANDA and ANEOS appear to be parallel to the melting curve (Fig. 4), and our Hugoniot temperature measurements are consistent with a smooth extension of ANEOS. Our P-d relation suggests that the melting in $CaCO_3$ is associated with a significant density increase (~7% higher than that of the crystal), contrasted with the melting of silicate.

There is another slope change in the increase of reflectivity and temperature starting at ~350 GPa (Fig. 3a). According to the Simon's melting curve, calcite becomes completely melted at this pressure. The reflectivity of $CaCO_3$ increases gradually with increasing pressure and becomes close to that of CO_2 around 800 GPa. Although there is no data available for CaO, the reflectivity might not be very low below ~500 GPa like MgO (Bolis et al., 2016; McCoy et al., 2019). If it is the case, the melt structure of $CaCO_3$ may change gradually. The measured temperatures in our study (Fig. 3b) show significantly below those for CO_2 in the pressure arrange between 300 GPa and 1000 GPa (Crandall et al., 2020). Simultaneous temperature measurements provide a way to calculate the isochoric specific heat C_v (Hicks et al., 2006).

$$C_v = [\Delta E_H - \Delta E_S]/[\Delta T_H - \Delta T_S]$$

where subscript S is along an isentrope, and H is along the Hugoniot. The result on the C_v calculation by the slope method (Hicks et al., 2006) is derived to be 2.5–2.8 kJ/kg • K between 340 and 960 GPa, which corresponds to 5.9–6.7 R (R: gas constant). Gruneisen parameter $\gamma = V(\delta P/\delta E)_v = 1.02$ is calculated at 960 GPa and 30000 K. The previous study on shocked SiO_2 reported the rapid rising of C_v/Nk_B (nondimensional specific heat, N is the number of atoms and k_B is Boltzmann's constant) from 3 (the Dulong-Petit limit) above the melting temperatures up to ~35000 K, indicating the melt with chemical bonds called as "bonded liquid" (Hicks et al., 2006). Similarly, we suppose that shocked calcite in our pressure range is also a bonded liquid up to 960 GPa and 30000 K. The large temperature deference between the present measurements and the previous calculations could be explained due to the bonded liquid state with enlarged specific heat by the reconfiguration reported as well as SiO_2 (Hicks et al., 2006; Millot et al., 2015; Knudson and Desjarlais, 2021). The transition pressure to the atomic fluid state of calcite is expected to be much higher than that of SiO_2 since the specific heat of calcite is higher than that of SiO_2. This may be related to the observed density increase (volume reduction) by melting of calcite at pressures over ~200 GPa (Fig. 2b).

4.2. Implications for planetary impacts and planetary interiors

From our study, the physical properties and the dynamic behaviors of shock-compressed and -released calcite at pressures of 200–1000 GPa are demonstrated to understand the high-velocity planetary impact phenomena at velocities exceeding 12 km/s (Zhang and Sekine, 2007). The precise Hugoniot measurements in this study enable us to estimate the released temperature of carbonates after impact events. At releasing from Hugoniot pressures of 100, 200, and 300 GPa (impact velocities of ~7, ~11, and ~ 14 km/s), the shocked calcite at the ambient condition will transform into the deferent phase of CaO (solid) + CO_2, CaO (liquid) + CO_2, or CaO (gas) + CO_2 respectively, as shown in Fig. 4 (Ivanov and Deutsch, 2002). Therefore, our results show that shock strength is critical for understanding the final phase of shocked products

with a planetary impact above 100 GPa. On the other hand, the calculation results on the released state indicate that CO_2 components as shock-induced products should be produced from impact events with carbonates above 100 GPa. This shock-induced CO_2 could play an important role in the formation processes of the planetary atmosphere.

Notably, we state that such complex reactions in calcite along the Hugoniot affect the estimation of the total energy of large-scale celestial collisions (e.g., ~200 km diameter in Chixulub impact crater) (Morgan et al., 1997; Morgan and Warner, 1999). If dissociation happens at extreme conditions like in the interiors of exoplanets and stars (Fortney, 2012; Teske et al., 2014), the present results also may imply a mechanism to change the ratio of C/O in the atmosphere composition.

According to the previous sample recovery experimental results, calcite degassed completely at shock pressures below 70 GPa, although there were some variations in the threshold pressure dependent on the starting material of single crystal/powders and encapsulated conditions of open/close system (e.g., onset and completed decomposition pressure; 10 GPa and 70 GPa by Lange and Ahrens, 1986; at 30–35 GPa and 45 GPa by Martinez et al., 1995; at 20 GPa and 33 GPa by Ohno et al., 2008, respectively). When calcite decomposes into CaO and CO_2 during the released process, the ratio of carbon monoxide to carbon dioxide (CO/CO_2) possibly depends on residual temperature. The CO/CO_2 from single-crystal calcite shocked at ~100 GPa was estimated to be about 0.1 (Kurosawa et al., 2012), and for porous calcite powders under similar experimental conditions, Kawaragi et al. (2009) reported that the average of CO/CO_2 is 2.0 at peak shock pressures from 17 to 90 GPa. Kurosawa et al. (2012) discussed that those 20 times deference in the CO/CO_2 ratio between both results came from the temperature difference due to different sample porosity (porosity: 8–17% in Kawaragi et al., 2009, vs. 0% in Kurosawa et al., 2012). These results show that the amount of CO generated from calcite increases with increasing temperature. CO is thermodynamically stable at high temperatures and the temperature in our experiments should be higher than those of previous studies (Kawaragi et al., 2009; Kurosawa et al., 2012) although the temperatures in these experiments have not been measured.

Finally, the results suggest the CO gas was produced significantly in large-scale planetary impacts more than previously estimated (Kawaragi et al., 2009; Kurosawa et al., 2012). CO production by intensive impacts can proceed efficiently in natural meteorites with high porosity (Bischoff et al., 2010). This fact may prompt a reconsidering of the estimation of the greenhouse effect and ocean temperature on the Earth. Moreover, the discussion for the effects of the turbulence of the expanded vapor and the various chemical reactions and the mixing of surrounding other minerals in post-shock clouds are also important to understand the final phase in the natural planetary impact phenomena.

The melting of calcite at high pressures shows a significant volume decrease (Fig. 2b) and the density is higher than that of crystal. Extrapolating U_s-u_p relations at low pressures below 100 GPa (corresponding to solid $CaCO_3$) and at high pressures over 200 GPa (liquid $CaCO_3$), the calculated densities at 150 GPa are 5.04 g/cm^3 and 5.49 g/cm^3, respectively. This is a contrast with those of silicates that show no detectable increase by melting (e.g, Bolis et al., 2016; Sekine et al., 2016). At relatively low pressures calcite melt has been investigated experimentally and theoretically, and such melts have lower densities than the crystal (Li et al., 2017; Zhang and Liu, 2015). The entropy jump (ΔS, J/K) of melting at high pressures should be also negative (the Clausius-Clapeyron relation $\Delta P/\Delta T = \Delta S/\Delta V$), suggesting higher coordination melt structures. This implies that calcite melts at extreme conditions may have distinct properties and that carbonate magmas in the lower mantle of the Earth and Super-Earths must be considered carefully after taking into account the present results. In the case of Earth, the experimental study using laser-heated diamond anvil cells reported that CO_4-based carbonates formed above 3000 K in the 100 GPa range may be carriers of carbon in the lower mantle (Cerantola et al., 2017). Understanding melt properties of mantle components of rocky planets allow us to propose concrete models for mantle convection, dynamo action, and planetary interiors (Stixrude, 2014; Soubiran and Militzer, 2018).

5. Conclusions

We determined the Hugoniot of single-crystal calcite at pressures of 200–960 GPa using laser shock compression techniques. Calcite becomes reflective above 200 GPa. The U_s-u_p relation is approximated by an equation of U_s (km/s) = (3.79 ± 0.33) + (1.26 ± 0.03) up (km/s), indicating a difference over 10% relative to the previous U_s-u_p by Kalashnikov et al. (1973). The temperature measurements using the decaying shock wave and the specific heat calculation suggest melting without decomposition at pressures of ~110 GPa to ~350 GPa and a bonded liquid state up to 960 GPa. The melting curve using Simon's equation was obtained as $T_m\ (K) = T_0\left(\frac{P(GPa)}{38.30}+1\right)^{0.69}$. Furthermore, the temperatures for calcite released from the Hugoniot indicated that the released products vary dependent on the Hugoniot pressure and the high-temperature reaction generated by high-velocity impacts may produce CO gas efficiently. The properties and structure of calcite melt in the present study is found to differ from those of silicate melts. The present results on calcite newly provide an important anchor for considering the theoretical EOS at the extreme conditions, where the model calculations show a significant diversity at present.

Declaration of Competing Interest

None.

Acknowledgments

Laser-shock experiments were conducted under the joint research project of the Institute of Laser Engineering, Osaka University. The authors thank Y. Kimura for her support with target fabrication. This work was supported by grants from MEXT Quantum Leap Flagship Program (MEXT Q-LEAP) grant no. JPMXS0118067246, Japan Society for the Promotion of Science (JSPS) KAKENHI (grant nos. 19K21866 and 16H02246), and Genesis Research Institute, Inc. (Konpon-ken, Toyota). T. Sekine acknowledges partial support by the National Natural Science Foundation of China (NSFC No. 41974099). This work was supported by the Future Development Funding Program of Kyoto University Research Coordination Alliance.

References

Amodeo, K.M., Davies, E.J., Stewart, S.T., Spaulding, D.K., 2021. Improving the SiO_2 equation of state with shock and post-shock temperatures. In: Proc. 52nd Lunar and Planetary Science Conference abstract no. 2714.
Anderson, O.L., 2000. The Grüneisen ratio for the last 30 years. Geophys. J. Int. 143, 279–294.
Barker, L.M., Hollenbach, R.E., 1972. Laser interferometer for measuring high velocities of any reflecting surface. J. Appl. Phys. 43, 4669–4775.
Barnes, J., Lyon, S., 1992. SESAME 7331 for Calcite : The Los Alamos National Laboratory Equation of State Database (LA-UR-92-3407).
Bischoff, A., Horstmann, M., Pack, A., Laubenstein, M., Haberer, S., 2010. Asteroid 2008 TC3−Almahata Sitta: a spectacular breccia containing many different ureilitic and chondritic lithologies. Meteorit. Planet. Sci. 45 (10−11), 1638–1656.
Boates, B., Hamel, S., Schwegler, E., Bonev, S.A., 2011. Structural and optical properties of liquid CO_2 for pressures up to 1 TPa. J. Chem. Phys. 134 (6), 064504.
Bolis, R.M., Morard, G., Vinci, T., Ravasio, A., Bambrink, E., Guarguaglini, M., Koenig, M., Musella, R., Remus, F., Bouchet, J., Ozaki, N., Miyanishi, K., Sekine, T., Sakawa, Y., Sano, T., Kodama, R., Guyot, F., Benuzzi-Mounaix, A., 2016. Decaying shock studies of phase transitions in MgO-SiO_2 systems: implications for the super-Earths' interiors. Geophys. Res. Lett. 43 (18), 9475–9483.
Celliers, P.M., Collins, G.W., Hicks, D.G., Eggert, J.H., 2005. Systematic uncertainties in shock-wave impedance-match analysis and the high- pressure equation of state of Al. J. Appl. Phys. 98, 113529.
Celliers, P.M., Loubeyre, P., Eggert, J.H., Brygoo, S., McWilliams, R.S., Hicks, D.G., Boehly, T.R., Jeanloz, R., Collins, G.W., 2010. Insulator-to-conducting transition in dense fluid helium. Phys. Rev. Lett. 104 (18), 184503.
Cerantola, V., Bykova, E., Kupenko, I., Merlini, M., Ismailova, L., McCammon, C., Bykov, M., Chumakov, A.I., Petitgirard, S., Kantor, I., Svitlyk, V., Jacobs, J.,

Hanfland, M., Mezouar, M., Prescher, C., Rüffer, R., Prakapenka, V.B., Dubrovinsky, L., 2017. Stability of iron-bearing carbonates in the deep Earth's interior. Nat. Commun. 8 (1), 1–9.
Crandall, L.E., Rygg, J.R., Spaulding, D.K., Boehly, T.R., Brygoo, S., Celliers, P.M., Eggert, J.H., Fratanduono, D.E., Henderson, B.J., Huff, M.F., Jeanloz, R., Lazicki, A., Marshall, M.C., Polsin, D.N., Zaghoo, M., Millot, M., Collins, G.W., 2020. Equation of state of CO_2 shock compressed to 1 TPa. Phys. Rev. Lett. 125 (16), 165701.
Daniel, J.S., Solomon, S., 1998. On the climate forcing of carbon monoxide. J. Geophys. Res. 103, 13249–13260.
Desjarlais, M.P., Knudson, M.D., Cochrane, K.R., 2017. Extension of the Hugoniot and analytical release model of α-quartz to 0.2-3 TPa. J. Appl. Phys. 122, 035903.
Eggert, J., Brygoo, S., Loubeyre, P., McWilliams, R.S., Celliers, P.M., Hicks, D.G., Boehly, T.R., Jeanloz, R., Collins, G.W., 2008. Hugoniot data for helium in the ionization regime. Phys. Rev. Lett. 100, 124503.
Fortney, J.J., 2012. On the carbon-to-oxygen ratio measurement in nearby sun-like stars: implications for planet formation and the determination of stellar abundances. Astrophys. J. Lett. 747 (2), L27.
Gulick, S.P.S., Barton, P.J., Christeson, G.L., Morgan, J.V., McDonald, M., Cervantes, K. M., Pearson, Z.F., Surendra, A., Fucugauchi, J.U., Vermeesch, P.M., Warner, M.R., 2008. Importance of pre-impact crustal structure for the asymmetry of the Chicxulub impact crater. Nat. Geosci. 1, 131–135.
Gupta, S.C., Love, S.G., Ahrens, T.J., 2002. Shock temperature in calcite ($CaCO_3$) at 95–160 GPa. Earth Planet. Sci. Lett. 201, 1–12.
Hicks, D.G., Boehly, T.R., Eggert, J.H., Miller, J.E., Celliers, P.M., Collins, G.W., 2006. Dissociation of liquid silica at high pressures and temperatures. Phys. Rev. Lett. 97 (2), 3–6. https://doi.org/10.1103/PhysRevLett.97.025502.
Irving, A.J., Wyllie, P.J., 1975. Subsolidus and melting relationship for calcite, magnesite and the join $CaCO_3$–$MgCO_3$ to 36 kb. Geochim. Cosmochim. Acta 39, 35–53.
Ivanov, B.A., Deutsch, A., 2002. The phase diagram of CaCO3 in relation to shock compression and decomposition. Phys. Earth Planet. Inter. 129 (1–2), 131–143.
Jeanloz, R., Ahrens, T.J., 1980. Equations of state of FeO and CaO. Geophys. J. Int. 62 (3), 505–528.
Kalashnikov, N.G., Pavlovskiy, M.N., Simakov, G.V., Trunin, R.F., 1973. Dynamic compressibility of calcite-group minerals. Izvestiya Phys. Solid Earth 2, 23–29.
Kargel, J.S., Kirk, R.L., Fegley Jr., B., Treiman, A.H., 1994. Carbonate-sulfate volcanism on Venus? Icarus 112 (1), 219–252.
Kawaragi, K., Sekine, Y., Kadono, T., Sugita, S., Ohno, S., Ishibashi, K., Kurosawa, K., Matsui, T., Ikeda, S., 2009. Direct measurements of chemical composition of shock-induced gases from calcite: an intense global warming after the Chicxulub impact due to the indirect greenhouse effect of carbon monoxide. Earth Planet. Sci. Lett. 282 (1–4), 56–64.
Kerley, G.I., 1989. Equations of state for calcite minerals. I. Theoretical model for dry calcium carbonate. High Pressure Res. 2 (1), 29–47.
Knudson, M.D., Desjarlais, M.P., 2009. Shock compression of quartz to 1.6 TPa: redefining a pressure standard. Phys. Rev. Lett. 103, 225501.
Knudson, M.D., Desjarlais, M.P., 2013. Adiabatic release measurements in α-quartz between 300 and 1200 GPa: characterization of α-quartz as a shock standard in the multimegabar regime. Phys. Rev. B 88, 184107.
Knudson, M.D., Desjarlais, M.P., 2021. Interplay of high-precision shock wave experiments with first-principles theory to explore molecular systems at extreme conditions: a perspective. J. Appl. Phys. 129, 210904.
Knudson, M.D., Lemke, R.W., Hayes, D.B., Hall, C.A., Deeney, C., Asay, J.R., 2003. Near-absolute Hugoniot measurements in aluminum to 500 GPa using a magnetically accelerated flyer plate technique. J. Appl. Phys. 94, 4420.
Kring, D.A., 1995. The dimensions of the Chicxulub impact crater and impact melt sheet. J. Geophys. Res. 100, 16979–16986.
Kurosawa, K., Ohno, S., Sugita, S., Mieno, T., Matsui, T., Hasegawa, S., 2012. The nature of shock-induced calcite ($CaCO_3$) devolatilization in an open system investigated using a two-stage light gas gun. Earth Planet. Sci. Lett. 337, 68–76.
Lange, M.A., Ahrens, T.J., 1986. Shock-induced CO_2 loss from $CaCO_3$; implications for early planetary atmosphere. Earth Planet. Sci. Lett. 77, 409–418.
Leuw, S., Rubin, A.E., Wasson, J.T., 2010. Carbonates in CM chondrites: complex formational histories and comparison to carbonates in CI chondrites. Meteorit. Planet. Sci. 45, 513–530.
Li, Z., Li, J., Lange, R., Liu, J., Militzer, B., 2017. Determination of calcium carbonate and sodium carbonate melting curves up to Earth's transition zone pressures with implications for the deep carbon cycle. Earth Planet. Sci. Lett. 457, 395–402.
Litvin, Y., Spivak, A., Solopova, N., Dubrovinsky, L., 2014. On origin of lower-mantle diamonds and their primary inclusions. Phys. Earth Planet. Inter. 228, 176–185.
Martinez, I., Deutsch, A., Schärer, U., Ildefonse, P., Guyot, F., Agrinier, P., 1995. Shock recovery experiments on dolomite and thermodynamical calculations of impact induced decarbonation. J. Geophys. Res. Solid Earth 100 (B8), 15465–15476.
McCoy, C.A., Marshall, M.C., Polsin, D.N., Fratanduono, D.E., Celliers, P.M., Meyerhofer, D.D., Boehly, T.R., 2019. Hugoniot, sound velocity, and shock temperature of MgO to 2300 GPa. Phys. Rev. B 100 (1), 014106.
Miller, J.E., Boehly, T.R., Melchior, A., Meyerhofer, D.D., Celliers, P.M., Eggert, J.H., Hicks, D.G., Sorce, C.M., Oertel, J.A., Emmel, P.M., 2007. Streaked optical pyrometer system for laser-driven shock-wave experiments on OMEGA. Rev. Sci. Instrum. 78 (3), 034903.
Millot, M., Dubrovinskaia, N.A., Cernok, A., Blaha, S., Dubrovinsky, L.S., Braun, D.G., Celliers, P.M., Collins, G.W., Eggert, J.H., Jeanloz, R., 2015. Shock compression of stishovite and melting of silica at planetary interior conditions. Science 347 (6220), 418. https://doi.org/10.1126/science.1261507.
Morgan, J., Warner, M., 1999. Chicxulub: the third dimension of a multi-ring basin. Geology 27, 407–410.
Morgan, J., Warner, M., Brittan, J., Buffler, R., Camargo, A., Christeson, G., Denton, P., Hildebrand, A., Hobbs, R., Macintyre, H., Mackenzie, G., Maguire, P., Marin, L., Nakamura, Y., Pilkington, M., Sharpton, V., Snyder, D., Suarez, G., Trejo, A., 1997. Size and morphology of the Chicxulub impact crater. Nature 390 (6659), 472–476.
Murchie, S.L., Mustard, J.F., Ehlmann, B.L., Milliken, R.E., Bishop, J.L., McKeown, N.K., Noe Dobrea, E.Z., Seelos, F.P., Buczkowski, D.L., Wiseman, S.M., Arvidson, R.E., Wray, J.J., Swayze, G., Clark, R.N., Des Marais, D.J., McEwen, A.S., Bibring, J.P., 2009. A synthesis of Martian aqueous mineralogy after 1 Mars year of observations from the Mars reconnaissance orbiter. J. Geophys. Res. 114 (E2), 1–30.
Ohno, S., Kadono, T., Ishibashi, K., Kawaragi, K., Sugita, S., Nakamura, E., Matsui, T., 2008. Direct measurements of impact devolatilization of calcite using a laser gun. Geophys. Res. Lett. 35 (13), 1–5.
O'Keefe, J.D., Ahrens, T.J., 1989. Impact production of CO_2 by the K/T extinction bolide and the resultant heating of the earth. Nature 338, 247–249.
Pierazzo, E., Kring, D.A., Melosh, H.J., 1998. Hydrocode simulation of the Chicxulub impact event and the production of climatically active gases. J. Geophys. Res. 103, 28607–28625.
Raikes, S.A., Ahrens, T.J., 1979. Post-shock temperatures in minerals. Geophys. J. R. Astron. Soc. 58, 717–747.
Sekine, T., 2011. 衝撃変成度の定量化に向けた展望. Yuseijin 20, 139–146. https://doi.org/10.14909/yuseijin.20.2_139.
Sekine, T., Kimura, T., Kobayashi, T., Mashimo, T., 2015. Dynamic water loss of antigorite by impact process. Icarus 250, 1–6.
Sekine, T., Ozaki, N., Miyanishi, K., Asaumi, Y., Kimura, T., Albertazzi, B., Sato, Y., Sakawa, Y., Sano, T., Sugita, S., Matsui, T., Kodama, R., 2016. Shock compression response of forsterite above 250 GPa. Sci. Adv. 2 (8), e1600157 https://doi.org/10.1126/sciadv.1600157.
Self, S., Widdowson, M., Thordarson, T., Jay, A.E., 2006. Volatile fluxes during flood basalt eruptions and potential effects on the global environment: a Deccan perspective. Earth Planet. Sci. Lett. 248 (1–2), 518–532.
Soubiran, F., Militzer, B., 2018. Electrical conductivity and magnetic dynamos in magma oceans of super-earths. Nat. Commun. 9 (1), 1–7.
Spivak, A.V., Dubrovinskii, L.S., Litvin, Y.A., 2011. Congruent melting of calcium carbonate in a static experiment at 3500 K and 10–22 GPa: its role in the genesis of Ultradeep diamonds. Dokl. Earth Sci. 439, 1171–1174.
Stixrude, L., 2014. Melting in super-earths. Philos. Trans. R. Soc. A Math. Phys. Eng. Sci. 372, 20130076.
Teske, J.K., Cunha, K., Smith, V.V., Schuler, S.C., Griffith, C.A., 2014. C/O ratios of stars with transiting hot Jupiter exoplanets. Astrophys. J. 788 (1), 39.
Wünnemann, K., Collins, G.S., Osinski, G.R., 2008. Numerical modeling of impact melt production in porous rocks. Earth Planet. Sci. Lett. 269, 530–539.
Zeldovich, Y.B., Raizer, Y.P., 1967. Physics of Shock Waves and High-Temperature Hydrodynamic Phenomena. Academic, New York.
Zhang, Z., Liu, Z., 2015. High pressure equation of state for molten CaCO3 from first principles simulations. Chin. J. Geochem. 31 (1), 13–20.
Zhang, F., Sekine, T., 2007. Impact-shock behavior of mg- and ca-sulfates and their hydrates. Geochim. Cosmochim. Acta 71, 4125.